ROYAL SOCIETY
OF CHEMISTRY

EDGE ARTICLE

Check for updates

All publication charges for this article
have been paid for by the Royal Society
of Chemistry

Charge-recombinative triplet sensitization of alkenes for DeMayo-type [2 + 2] cycloaddition†

Yunjeong Lee,‡[a] Byung Hak Jhun,‡[b] Sihyun Woo,‡[c] Seoyeon Kim,[a] Jaehan Bae,[a] Youngmin You [ID] *[b] and Eun Jin Cho [ID] *[a]

Synthetic photochemistry has undergone significant development, largely owing to the development of visible-light-absorbing photocatalysts (PCs). PCs have significantly improved the efficiency and precision of cycloaddition reactions, primarily through energy or electron transfer pathways. Recent research has identified photocatalysis that does not follow energy- or electron-transfer formalisms, indicating the existence of other, undiscovered photoactivation pathways. This study unveils an alternative route: a charge-neutral photocatalytic process called charge-recombinative triplet sensitization (CRTS), a mechanism with limited precedents in synthetic chemistry. Our investigations revealed CRTS occurrence in DeMayo-type [2 + 2] cycloaddition reactions catalyzed by indole-fused organoPCs. Our mechanistic investigations, including steady-state and transient spectroscopic analyses, electrochemical investigations, and quantum chemical calculations, suggest a mechanism involving substrate activation through photoinduced electron transfer, followed by charge recombination, leading to substrate triplet state formation. Our findings provide valuable insights into the underlying photocatalytic reaction mechanisms and pave the way for the systematic design and realization of innovative photochemical processes.

Introduction

Photochemical cycloaddition belongs to a versatile chemical reaction class that harnesses photon energy to form cyclic compounds, playing a significant role in organic chemistry.[1–8] It enables the synthesis of a wide range of compounds with precise control over regio- and stereoselectivity. Historically, photochemical cycloadditions have been achieved through stoichiometric photon absorption by substrates with certain π conjugations, such as alkenes (Fig. 1a). In the past one and a half decades, synthetic photochemistry has experienced a remarkable resurgence, driven largely by the development of visible-light-absorbing photocatalysts (PCs).[9–13] PC introduction has substantially enhanced the efficiency and enantioselectivity of cycloaddition processes, primarily through charge-neutral energy transfer (EnT) (Fig. 1b).[14–20] Another common approach is photoredox catalytic cycloaddition, where the electron

transfer (ET) pathway generates key radical intermediates (Fig. 1c).[21–26] The critical factor for successful EnT and ET processes is the exergonicity determined by the excited-state energies and redox potentials, respectively, of the PC and the organic substrate.[27–30] However, in some cases, PCs have exhibited satisfactory catalytic performance despite noticeable mismatches in energetic or electrochemical conditions.[31] This observation suggests the existence of alternative, uncharted photoactivating pathways.

In this study, we investigated an alternative route: charge-neutral photocatalytic process *via* charge-recombinative triplet sensitization (CRTS), a mechanism with limited precedents in synthetic chemistry (Fig. 1d).[32,33] To investigate this uncommon CRTS mechanism, we utilized an indole-based polycyclic organoPC series,[34,35] developed in our laboratory, for a DeMayo-type [2 + 2] cycloaddition[36–44] between methyl-2-(quinolin-2-yl)acetate (**1**) and various styrene derivatives. Detailed studies involving photophysical and electrochemical measurements and computational analyses provide insights into this unique CRTS pathway.

[a]*Department of Chemistry, Chung-Ang University, 84 Heukseok-ro, Dongjak-gu, Seoul 06974, Republic of Korea. E-mail: ejcho@cau.ac.kr*

[b]*Department of Chemical and Biomolecular Engineering, Yonsei University, 50 Yonsei-ro, Seodaemun-gu, Seoul 03722, Republic of Korea. E-mail: odds2@yonsei.ac.kr*

[c]*Division of Chemical Engineering and Materials Science, Ewha Womans University, 52 Ewhayeodae-gil, Seodaemun-gu, Seoul 03760, Republic of Korea*

† Electronic supplementary information (ESI) available. CCDC 2225142. For ESI and crystallographic data in CIF or other electronic format see DOI: https://doi.org/10.1039/d4sc02601b

‡ These authors contributed equally.

Results and discussion

Photocatalytic DeMayo-type [2 + 2] cycloaddition reactions

Our investigation began with screening various PCs for the DeMayo-type reaction between model substrates, **1** and styrene (**2a**) (Table 1). We employed indole-fused polycyclic organoPCs
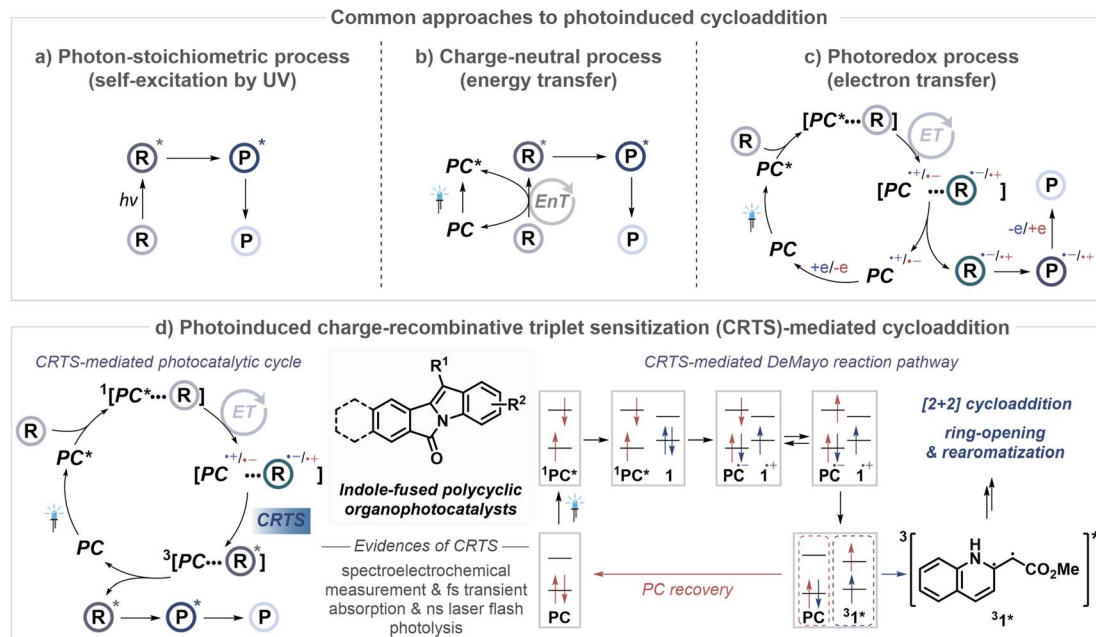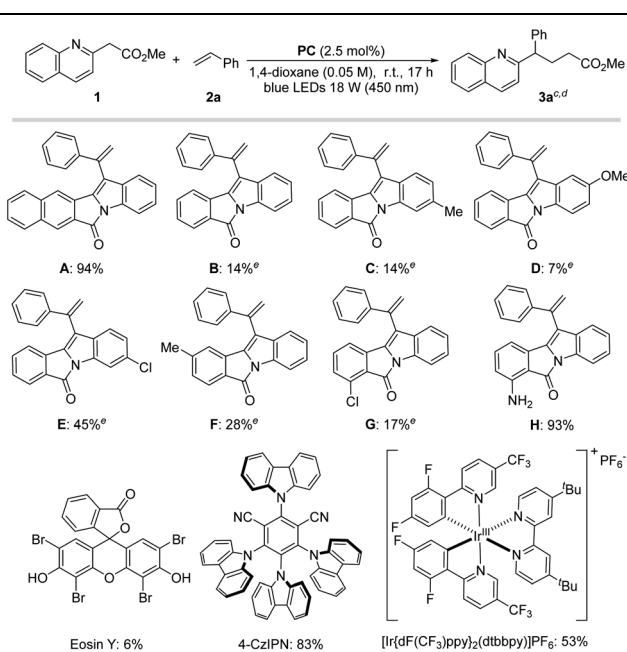
Fig. 1   Photoinduced cycloaddition.

Table 1 Photocatalyst screening in DeMayo-type [2 + 2] cycloadditions[a,b]

[a] Reaction scale: **1** (0.1 mmol), **2a** (0.5 mmol) under an Ar atmosphere. [b] The yield was determined by ¹H NMR spectroscopy using 1,3,5-trimethoxybenzene as an internal standard. [c] Yield of **3a**: 0% (without PC). [d] Yield of **3a**: 0% (without light, with **A**). [e] **1** and **2a** remain unreacted.

(**A–H**) (2.5 mol%) in 1,4-dioxane under visible light irradiation, utilizing 18 W blue light-emitting diodes (LEDs) for the formation of **3a**.[45] Our systematic investigations revealed that structural variations in the PCs substantially impacted catalytic

activity. Among the tested organoPCs, the pentacyclic organoPC **A** (CCDC 2225142; see Fig. S1†) and an amino-substituted tetracyclic variant **H** exhibited reactivity superior to those of the remaining tetracyclic systems.

In addition to our indole-fused organoPCs, we also evaluated widely used PCs such as Eosin Y, 4-CzIPN, and [Ir{dF(CF₃)ppy}₂(dtbbpy)]PF₆.[41] However, none of these PCs exhibited superior reactivity compared to **A** and **H**. Control experiments showed that in the absence of an organoPC or visible light, the reaction did not proceed at all, confirming its photocatalytic nature.

The quantum yield for the reaction of **1** and **2a**, which was determined using the standard ferrioxalate actinometry, is 49% with **A** and 48% with **H**. The other photocatalysts show quantum yields for the reaction in the range 4–23% (Table S1†). The values lower than 100% suggest the absence of intermediacy of any chain reaction.

Mechanistic investigations of photocatalytic DeMayo-type [2 + 2] cycloaddition reactions

Subsequently, our focus shifted toward understanding the photocatalytic process mechanism, particularly the origin of the superior reactivity of **A** and **H**. In the DeMayo-type [2 + 2] cycloaddition reaction, substrate triplet sensitization is a critical step.[36,40–42,44] Thus, our investigation emphasized elucidating how indole-based polycyclic organoPCs facilitate photosensitization that leads to the generation of the substrate triplet state.

First, the photoluminescence (fluorescence) spectra were recorded for Ar-saturated 1,4-dioxane containing 1.0 mM **A** and increasing concentrations of **1** (0–500 mM) under 345 nm photoexcitation. As shown in Fig. 2a, the photoluminescence intensity of **A** decreased with increasing **1** concentration,
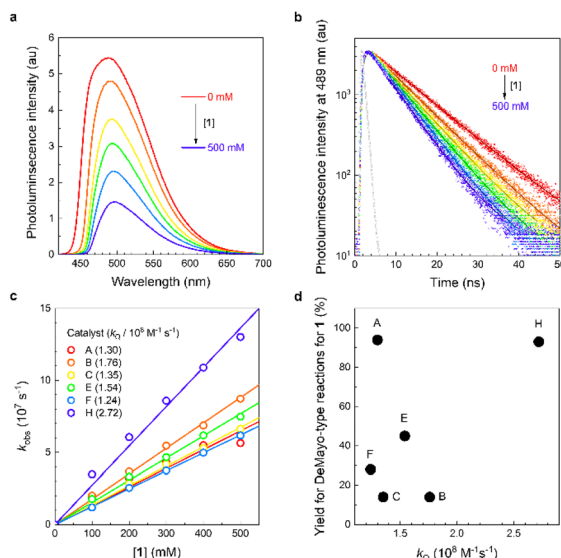
Fig. 2 Excited state interactions. (a) Photoluminescence (fluorescence) spectra of 1.0 mM **A** containing increasing concentrations of **1** in deaerated 1,4-dioxane. (b) Photoluminescence decay traces of 1.0 mM **A** in deaerated 1,4-dioxane, recorded after pulsed 345 nm laser photoexcitation at increasing **1** concentrations. (c) Corresponding quenching rate constant, $k_{obs} = 1/\tau_{obs}(\mathbf{1}) - 1/\tau_{obs}(0)$, as a function of **1** concentration, where $\tau_{obs}(\mathbf{1})$ and $\tau_{obs}(0)$ are photoluminescence lifetimes of **A** in the presence and absence of **1**. Values are the rate constants for hetero-bimolecular quenching (k_Qs) of organoPCs by **1**. (d) Yield of DeMayo-type [2 + 2] cycloaddition of **1** as a function of k_Q.

suggesting a nonradiative interaction between **1** and excited state **A** (**A***). The quenching interaction hardly required a ground-state association between the two species, as seen from the decreasing photoluminescence lifetime (τ_{obs}) of **A*** without a multiphasic transition in the decay trace (Fig. 2b; see Fig. S2† for results for the other organoPCs, **B**–**H**). The photoluminescence quenching rate constant (k_{obs}) is estimated from

the relationship: $k_{obs} = 1/\tau_{obs}(\mathbf{1}) - 1/\tau_{obs}(0)$, where $\tau_{obs}(\mathbf{1})$ and $\tau_{obs}(0)$ are τ_{obs} in the presence and absence, respectively, of **1**; the k_{obs} increases with the molar concentration of **1** ([**1**]), consistent with bimolecular quenching.

Pseudo-first-order kinetic analyses of k_{obs} yielded the rate constant for hetero-bimolecular quenching (k_Q) of **A**–**H** in the range of 1.2–2.7×10^8 M^{-1} s^{-1}, which approaches the diffusion-limited regime in 1,4-dioxane at 298 K (Fig. 2c and Table 2). Notably, k_Q does not correlate with the yield of the DeMayo-type [2 + 2] cycloaddition reactions of **1** (Fig. 2d), which suggests that the quenching of excited-state organoPCs by the substrate is not a rate-determining step in the overall photocatalytic cycle.

The quenching of **A*** by **1** does not result from EnT. We found that k_Q exhibited a poor proportional relationship with the spectral overlap integral (J) between the UV-Vis absorption spectrum of **1** and the photoluminescence spectrum of **A** (Fig. S3 and S4†). The absence of proportionality indicates that the interaction between **A*** and **1** does not originate from singlet–singlet EnT that follows the Förster formalism. Moreover, the photoluminescence quenching behaviors are inconsistent with Förster EnT theories (see Fig. S5† for further discussion). In addition, even though the singlet sensitization of **1** to its excited state ($^1\mathbf{1}^*$) by the organoPCs would take place, $^1\mathbf{1}^*$ is unlikely to be converted to its triplet state ($^3\mathbf{1}^*$); our quantum calculations, based on the method of Ma et al.,[46] indicate negligibly low rates (k_{ISC}s) for intersystem crossing (ISC): 1.4×10^2 s^{-1} for the benzenoid form and 2.7×10^3 s^{-1} for the quinoid form of **1** (Table S2†). These results support the hypothesis that singlet–singlet EnT is not a productive pathway. Furthermore, the formation of an EDA complex and an exciplex can be excluded based on the absence of new bands in the UV-Vis absorption and photoluminescence spectra of a mixture of **A** and **1** or **2a** (Fig. S6 and S7†).

In contrast, our femtosecond and nanosecond transient absorption spectroscopy experiments revealed a relatively fast ISC for the organoPCs, occurring at a rate of $k_{ISC} = 0.63$–$10 \times$

Table 2 Photophysical and kinetic parameters of PCs and **1**

	λ_{abs}^a (nm, $\varepsilon/10^4$ M^{-1} cm^{-1})	E_{S1}^b (eV)	λ_{em}^c (nm)	τ_{obs}^d (ns)	Φ_{PL}^e	k_r^f (10^7 s^{-1})	k_{nr}^g (10^7 s^{-1})	k_{ISC}^h (10^7 s^{-1})	J^i (10^{12} M^{-1} cm^{-1} nm^4)	k_Q^j (10^8 M^{-1} s^{-1})	k_{PeT}^k (10^8 M^{-1} s^{-1})	k_{CR}^l (10^8 M^{-1} s^{-1})
A	294 (4.40)	2.74	489	11	0.21	2.0	7.5	1.7	1.5	1.3	1.3	6.9
B	303 (1.29)	2.86	484	8.8	0.20	2.3	9.1	—	6.2	1.8	1.8	0.66
C	290 (1.88)	2.78	491	10	0.25	2.6	7.7	0.63	1.2	1.4	1.4	1.8
D	302 (2.00)	2.93	539	1.2	0.0045	0.37	83	—	—	—	—	0.66
E	290 (1.39)	2.83	479	12	0.47	4.0	4.6	—	2.5	1.5	1.6	1.9
F	290 (1.43)	2.85	478	8.9	0.21	2.3	8.9	10	2.0	1.2	1.3	3.8
G	378 (1.38)	2.81	486	8.5	0.23	2.7	9.1	—	—	—	—	4.1
H	412 (1.57)	2.73	462	3.4	0.39	11	18	1.0	2.7	2.7	2.9	9.3
1	316 (0.42)	2.69	365	—	—	—	—	—	—	—	—	—

^{a} Absorption peak wavelength (molar absorbance). ^{b} The first singlet state energy was determined from the UV-Vis absorption spectra onset wavelengths. ^{c} Emission peak wavelength. ^{d} Photoluminescence lifetime determined through nonlinear least-squares fitting to a mono-exponential decay model of decay traces after picosecond pulsed 345 nm excitation. ^{e} Photoluminescence quantum yield was determined using 9,10-diphenylanthracene as a standard (toluene, $\Phi_{PL} = 1.00$). ^{f} Radiative rate constant, $k_r = \Phi_{PL}/\tau_{obs}$. ^{g} Nonradiative rate constant, $k_{nr} = (1 - \Phi_{PL})/\tau_{obs}$. ^{h} Intersystem crossing rate. ^{i} Spectral overlap is integral between the absorption spectrum of the substrate and the photocatalyst emission spectrum. ^{j} The bimolecular quenching rate constant was determined from pseudo-first-order kinetic analyses of the photocatalyst fluorescence quenching rates with the substrate. ^{k} The rate constant for the bimolecular photoinduced electron transfer rate was determined through the relationship $k_{PeT} = -(k_Q \times k_{diff})/(k_Q - k_{diff})$, where k_{diff} is the 1,4-dioxane diffusion rate constant at 298 K, estimated from the Stokes–Einstein–Smoluchowski equation. ^{l} The rate constant for charge recombination within the radical ion pair [**PC**$^{•-}$···**1**$^{•+}$] to form $^3\mathbf{1}^*$.
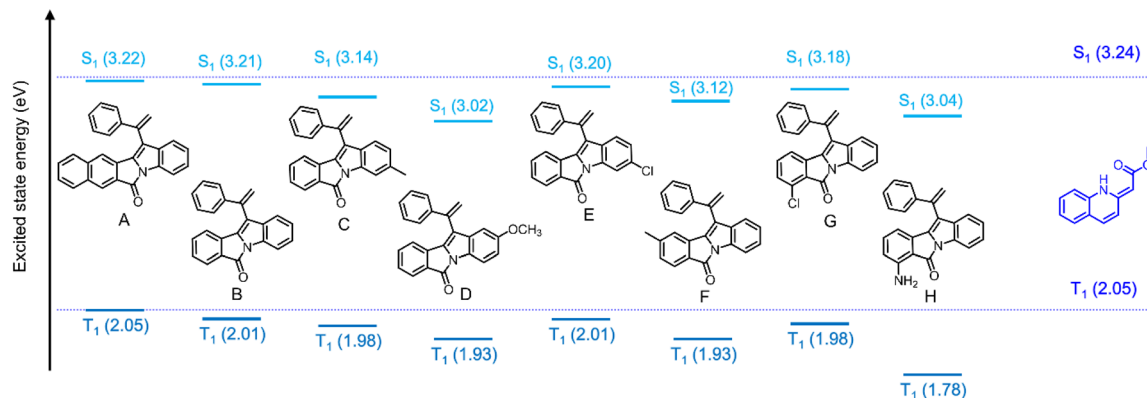
Fig. 3 Energy level alignments. Singlet (S_1) and triplet (T_1) state energies of organoPCs **A–H** and the quinoid form of **1**, calculated at the w-B97X-D/TZP//B3LYP-D3(BJ)/TZP level using a solvation method based on the conductor-like screening model parameterized for 1,4-dioxane.

10^7 s^{-1} (Fig. S8† and Table 2). The ISC of **A** occurs at a rate (k_{ISC} = 1.7×10^7 s^{-1}) twice as fast as its k_{obs} in the presence of 0.050 M **1** (*i.e.*, 6.5×10^6 s^{-1} = 1.3×10^8 M^{-1} s^{-1} × 0.050 M). Based on the ISC behavior, one might consider that **1** undergoes triplet sensitization through consecutive processes involving the ISC of an organoPC, followed by triplet–triplet EnT from the organoPC triplet state to **1**. However, quantum chemical calculations at the B3LYP-D3(BJ) level of theory using the TZP basis set, followed by time-dependent w-B97X-D calculations considering solvation effects, contradict this scenario. As shown in Fig. 3, the triplet (T_1) states of the **B–H** ground-state geometries (1.78–2.01 eV) were located below the T_1 state of the quinoid form of the **1** ground state (2.05 eV). In particular, the significant T_1 state energy difference between **H** and **1** (0.27 eV) strongly indicates that substrate activation *via* triplet–triplet EnT is unfavorable, except for **A**. Notably, **H** catalyzes the DeMayo reaction of **1**, with yields as high as 93%. In the case of **A**, its T_1 state is isoenergetic with the T_1 state of **1** (2.05 eV). Our quantum chemical calculations for **1** reveal localization of the spin density within the heterocycle and methyne units (Fig. S9†), which suggests an occurrence of the [2 + 2] cycloaddition reaction with **2a**, but refutes the possibility for the [4 + 2] cycloaddition.[47] In addition, the singlet excited (S_1) states of the **A–H** ground-state geometries (3.02–3.22 eV) are predicted to be lower in energy than the S_1 state of the quinoid form of **1** (3.24 eV). These energetic alignments indicate that EnTs from the excited-state organoPCs to **1** are endoergic, suggesting that triplet sensitization of **1** *via* EnT is not feasible.

The Dexter theory of electron exchange predicts that the process rate decreases exponentially with increasing distance between the catalyst and the substrate. Good linearity was observed between the logarithm of the photoluminescence quenching rate constant, k_{obs}, and $[1]^{-1/3}$ (Fig. S5b†). This adherence to Dexter formalism implies that an excited-state organoPC is quenched by unidirectional or bidirectional ET—that is, the formation of a radical ion pair or EnT, respectively. Because EnT has been refuted, it is tempting to assert that unidirectional, photoinduced hetero-bimolecular ET forms radical ion pairs of the organoPC and substrate. To examine this possibility, we determined the oxidation (E_{ox}) and reduction

(E_{red}) potentials of **A–H** and **1** using cyclic and differential pulse voltammetry (Fig. S10 and S11†). The excited-state redox potentials of organoPCs were subsequently calculated from the relationships $E_{ox}^* = E_{ox} - E_{S1}$ and $E_{red}^* = E_{red} + E_{S1}$, where E_{ox}^* is the excited-state oxidation potential, E_{S1} is the S_1 state energy determined from the onset wavelength of the UV-Vis absorption spectrum, and E_{red}^* is the excited-state reduction potential. The ground- and excited-state redox potentials are compiled in Table 3. The E_{ox}^* (−1.52–1.37 V *vs.* standard calomel electrode (SCE)) of **A–H** are found to be more cathodic than the E_{red} (−1.13 V *vs.* SCE) of the **1** quinoid form. This electrochemical disposition allows photoinduced ET from organoPCs to **1**, forming a geminate radical ion pair consisting of a one-electron oxidized species of organoPC (denoted as **PC**$^{\cdot+}$) and a one-electron reduced form of **1** (denoted as **1**$^{\cdot-}$). The driving force for the oxidative quenching of excited-state organoPC ($-\Delta G_{PeT}^{ox}$) can be estimated from the relationship $-\Delta G_{PeT}^{ox} = e[E_{ox}^*(\mathbf{PC}) - E_{red}(\mathbf{1})]$, where e is the elementary charge; $E_{ox}^*(\mathbf{PC})$ is the E_{ox}^* of an organoPC; and $E_{red}(\mathbf{1})$ is the E_{red} of **1**. The Coulomb term was ignored in this estimation owing to the use of polar 1,4-dioxane. The $-\Delta G_{PeT}^{ox}$ spans the range 0.24–0.39 eV (Table 3), which indicates that the oxidative quenching of **A–H** by **1** is exergonic. In addition to oxidative quenching, the reductive quenching of **A–H** to form a geminate radical ion pair of the organoPC radical anion (**PC**$^{\cdot-}$) and the **1** radical cation (**1**$^{\cdot+}$) is thermodynamically allowed. The driving force for the reductive quenching ($-\Delta G_{PeT}^{red}$), estimated from the relationship $-\Delta G_{PeT}^{red} = e[E_{ox}(\mathbf{1}) - E_{red}^*(\mathbf{PC})]$ where $E_{ox}(\mathbf{1})$ and $E_{red}^*(\mathbf{PC})$ are E_{ox} of **1** and the excited-state reduction potential of an organoPC, respectively, is in the range 0.31–0.55 eV (Table 3). Taken together, our electrochemical analyses suggest the formation of radical ion pairs of [**PC**$^{\cdot+}$⋯**1**$^{\cdot-}$] or [**PC**$^{\cdot-}$⋯**1**$^{\cdot+}$]. To monitor the radical ion pairs directly, we performed nanosecond laser flash photolysis (LFP) experiments on Ar-saturated 1,4-dioxane containing 1.0 mM **A** and 100 mM **1**. The mixture was photo-irradiated under nanosecond pulsed laser excitation at 355 nm. As shown in Fig. 4a, a weak photoinduced absorption (PIA) signal emerged at wavelengths greater than 800 nm, together with significant photoinduced bleaching (PIB) in the shorter wavelength region due to the stimulated emission of **A***. The PIA spectrum

Table 3 The T_1 state energies, electrochemical potentials, and the driving forces for photoinduced electron transfer and charge recombination between the photocatalyst and **1**

	E_{T1}^{a} (eV)	E_{ox} (V vs. SCE)	E_{red} (V vs. SCE)	$E_{ox}^{*\ b}$ (V vs. SCE)	$E_{red}^{*\ c}$ (V vs. SCE)	$-\Delta G_{PeT}^{ox\ d}$ (eV)	$-\Delta G_{PeT}^{red\ e}$ (eV)	$-\Delta G_{CR}^{f}$ (eV)	$-\Delta G_{CR}^{*\ g}$ (eV)
A	2.05	1.37	−1.50	−1.37	1.24	0.24	0.35	2.39	0.34
B	2.01	1.47	−1.42	−1.39	1.44	0.26	0.55	2.31	0.26
C	1.98	1.38	−1.45	−1.40	1.33	0.27	0.44	2.34	0.29
D	1.93	—	—	—	—	—	—	—	—
E	2.01	—	—	—	—	—	—	—	—
F	1.93	1.44	−1.46	−1.41	1.39	0.28	0.50	2.35	0.30
G	1.98	—	—	—	—	—	—	—	—
H	1.78	1.21	−1.53	−1.52	1.20	0.39	0.31	2.42	0.37
1	2.05	0.89	−1.13	−1.80	1.56	—	—	—	—

^{a} The T_1 state energies of the photocatalysts were calculated at the w-B97X-D/TZP//B3LYP-D3(BJ)/TZP level with COSMO parameterized for 1,4-dioxane. ^{b} Excited-state oxidation potential, $E_{ox}^{*} = E_{ox} - E_{S1}$. ^{c} Excited-state reduction potential, $E_{red}^{*} = E_{red} + E_{S1}$. Table 2 presents the E_{S1} values of the samples. ^{d} Driving force for oxidative electron transfer from the excited-state catalyst to **1**, $-\Delta G_{PeT}^{ox} = e[E_{ox}^{*}(PC) - E_{red}(1)]$. ^{e} Driving force for reductive electron transfer from **1** to the excited-state organoPC, $-\Delta G_{PeT}^{red} = e[E_{ox}(1) - E_{red}^{*}(PC)]$. ^{f} Driving force for the charge recombination reaction, $PC^{\cdot-} + 1^{\cdot+} \rightarrow PC + 1$, $-\Delta G_{CR} = e[E_{ox}(1) - E_{red}(PC)]$. ^{g} Driving force for the charge recombination reaction, $PC^{\cdot-} + 1^{\cdot+} \rightarrow PC + {}^3 1^*$, $-\Delta G_{CR}^{*} = -\Delta G_{CR} - E_{T1}(1)$.

consisted of bands with approximately 840 and 1400 nm peak wavelengths.

On the other hand, the spectrum of the control solution devoid of **1** exhibited negligible PIA bands in the range 1200–1600 nm. The PIA band at 1400 nm coincides with the visible-NIR absorption spectrum of $A^{\cdot-}$ electrochemically generated at −2.0 V vs. $Ag^{+/0}$ (ε at 1400 nm is 285 M^{-1} cm^{-1}). The simulated UV-Vis-NIR absorption spectrum of $A^{\cdot-}$ further supports these observations (the fourth panel in Fig. 4a). These results provide compelling evidence for the photoinduced formation of $[A^{\cdot-} \cdots 1^{\cdot+}]$.

Once formed, the radical ion pair $[A^{\cdot-} \cdots 1^{\cdot+}]$ rapidly disappears through charge recombination via back-ET from $A^{\cdot-}$ to $1^{\cdot+}$ within the solvent cage. Note that $1^{\cdot+}$ or its resonance benzylic radical derivative might react with the alkene; however, we excluded this pathway because it cannot lead to DeMayo-type [2 + 2] cycloaddition, which should occur through biradical intermediates (see Fig. S9 and Table S17†). This charge recombination typically produces charge-neutral ground-state species (that is, **A** and **1**). When the driving force for charge recombination ($-\Delta G_{CR}$) is greater than the constituent species T_1 state energy, charge recombination sensitizes the triplet state. We have previously reported CRTS in organic light-emitting devices[48,49] and photoredox catalysis.[50] The $-\Delta G_{CR}$ for $[A^{\cdot-} \cdots 1^{\cdot+}]$ amounts to 2.39 eV, as estimated by $-\Delta G_{CR} = e[E_{ox}(1) - E_{red}(A)]$. This $-\Delta G_{CR}$ value is greater than the T_1 state energy (2.05 eV) of the quinoid form of **1** (Fig. 3 and Table 3). The corresponding driving force for charge-recombinative sensitization ($-\Delta G_{CR}^{*}$) of $^3 1^*$ is estimated to be 0.34 eV for **A** from the relationship $-\Delta G_{CR}^{*} = -\Delta G_{CR} - E_{T1}(1)$. Although we could not directly observe the spectroscopic signatures of $^3 1^*$, presumably because of its weak signals, the positive $-\Delta G_{CR}^{*}$ indicates the spontaneity of the CRTS of $^3 1^*$. The $-\Delta G_{CR}^{*}$ values for **A–H** are in the range 0.26–0.37 eV (Table 3).

The question remains as to why **A–H** produce different yields in DeMayo-type [2 + 2] cycloaddition reactions (Table 1). These differences may originate from their different rates of charge-recombinative substrate triplet sensitization. We determined the charge recombination rate (k_{CR}) through second-order kinetic analyses of the $A^{\cdot-}$ PIA decay traces, which were recorded at a wavelength of 1400 nm using the molar absorbance determined spectrophotometrically ($\varepsilon = 285$ M^{-1} cm^{-1}) (Fig. 4b). k_{CR} was determined to be as large as 6.9×10^8 M^{-1} s^{-1} for $A^{\cdot-}$ and $1^{\cdot+}$. The k_{CR} values for the other organoPCs, **B–H**, were also determined (Table 2). As shown in Fig. 4c, k_{CR} increases with $-\Delta G_{CR}^{*}$. Based on the Jortner ET formalism,[49] our analyses suggest that charge recombination occurs in the Marcus normal region of ET with a reorganization energy of 1.2 eV. More importantly, a mild linear relationship was observed between k_{CR} and the yield for the DeMayo-type [2 + 2] cycloaddition reaction (Fig. 4d). For instance, **A** and **H**, which had the largest k_{CR} values, produced the best catalytic performance, whereas **D**, which had the smallest k_{CR}, elicited the lowest reaction yield. Although inconclusive, the linearity strongly suggests that charge recombination, which generally causes quenching of the reaction, is actually a key step in our results. Therefore, it can be concluded that the charge-
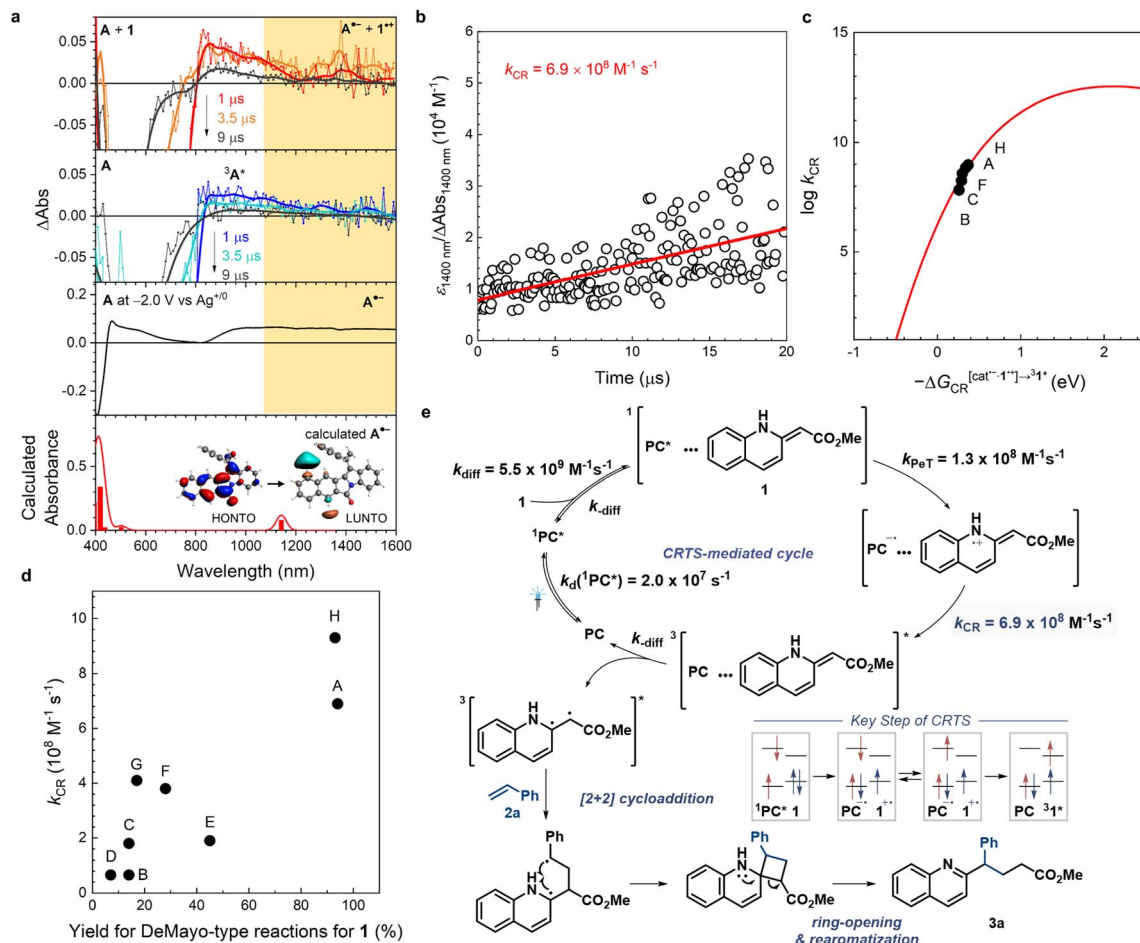
Fig. 4 Photoinduced charge separation and charge-recombinative triplet sensitization (CRTS). (a) Nanosecond transient absorption spectra of 1.0 mM **A** in the presence (top-most panel) and absence (second panel) of 100 mM **1** recorded at 1, 3.5, and 9 μs after pulsed 355 nm laser excitation (temporal resolution = 80 ns; laser power = 580 mW). The negative ΔAbs signals in the range 420–640 nm were due to the stimulated emission of **A**. The third panel shows UV-Vis-NIR absorption difference spectra of 2.0 mM **A** (Ar-saturated DMF containing 0.10 M TBAPF$_6$) recorded with an applied cathodic potential of −2.0 V vs. Ag$^{+/0}$. A Pt mesh and Pt wire were used as the working and counter electrodes, respectively. An Ag/AgNO$_3$ pseudo-reference electrode was used in this study. The area highlighted in yellow indicates absorption due to **A**$^{•−}$. The fourth panel shows the simulated UV-Vis-NIR spectrum of **A**$^{•−}$ calculated at the unrestricted wB97X-D/TZP//B3LYP-D3(BJ)/TZP level of theory with the COSMO parameterized for 1,4-dioxane. (b) Second-order kinetic analyses of decay traces of **A**$^{•−}$ recorded at a wavelength of 1400 nm. (c) Log k_{CR} as a function of the driving force for the reaction PC$^{•−}$ + **1**$^{•+}$ → PC + ^{3}**1*** ($−\Delta G^*_{CR}$). The red curve is the theoretical curve predicted by the Jortner formalism, with a reorganization energy of 1.2 eV. (d) Plot of k_{CR} as a function of yield for DeMayo-type [2 + 2] cycloaddition reactions for **1**. (e) Plausible mechanism. These values were determined for **A**.

recombinative triplet-state generation step governs the overall catalytic performance.

Based on these results, we propose a plausible mechanism involving **1** and **2a** (Fig. 4e). Because the DeMayo-type [2 + 2] cycloaddition proceeds from the T$_1$ state, substrate triplet activation is essential. Our proposed mechanism involves a photoinduced cycle of consecutive steps, including (i) initial photon absorption by an organoPC to form an excited-state organoPC (^{1}**PC***) that is intrinsically deactivated at a rate of 2.0 × 10^7 s^{-1} in the case of **A**; (ii) diffusion-controlled formation of an encounter complex between ^{1}**PC*** and a substrate [^{1}**PC***···substrate];[51] (iii) ET from the substrate to ^{1}**PC*** to form a radical ion pair [**PC**$^{•−}$···substrate$^{•+}$]; (iv) charge recombination within the radical ion pair to form the substrate T$_1$ state; (v) dissociation of the triplet substrate and the **PC**. The triplet substrate

subsequently reacts with styrene **2a** to generate a biradical adduct, or the biradical intermediate may cyclize readily to form a cyclobutane intermediate. Finally, ring-opening[52] followed by aromatization produces **3a**.

Substrate scope

Next, the reaction scope was investigated using a range of alkene derivatives (**2**) under optimized reaction conditions (Table 4). Various styrene derivatives underwent regioselective DeMayo-type [2 + 2] cycloadditions to yield the corresponding ring-opening and aromatization products (**3a–3t**) irrespective of the electron density or position (*ortho-*, *meta-*, *para-*) of the substituents on the aromatic ring. The mild reaction conditions tolerated functional groups, including chloride (**3j**, **3o**) and bromide (**3k**); medicinally important F (**3l**, **3m**)[53–55] substituents

Table 4 Substrate scope^{a,b}
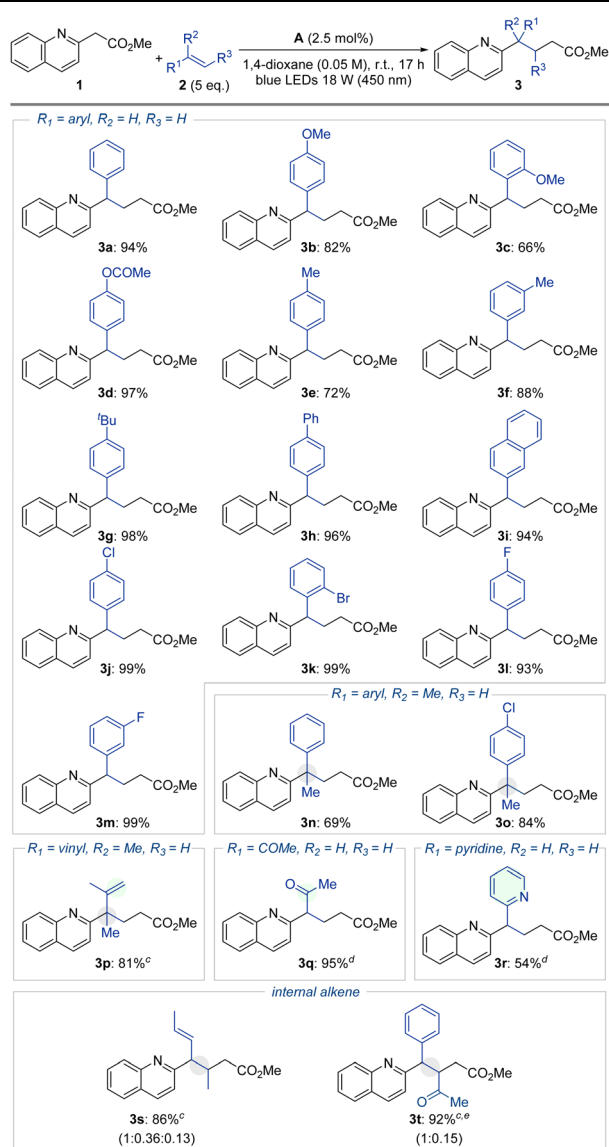
^{a} Reactions were performed on a 0.3 mmol scale. ^{b} Isolated yields are reported. ^{c} Reaction time: 24 h. ^{d} Reaction time: 48 h. ^{e} **2t** (1 eq.).

could also be used, and a heteroaryl variant, the pyridine-substituted (**3r**) derivative, was also suitable for the transformation. Notably, nonaromatic (**3p**, **3q**, **3s**) and internal alkenes (**3s**, **3t**) were also suitable coupling partners under the standard conditions. However, simple aliphatic alkenes lacking the ability to form resonance-stabilized radical intermediates were ineffective in this transformation (see Fig. S14†).

Conclusions

In summary, our investigation explored the uncharted territory of the CRTS process in DeMayo-type [2 + 2] cycloaddition reactions using indole-fused organoPCs developed in our laboratory. The intricate mechanism involves substrate activation through photoinduced ET, followed by charge recombination

that leads to substrate triplet state generation. Comprehensive steady-state and transient spectroscopic experiments, electrochemical investigations, and quantum chemical calculations validated this mechanism. Our findings not only shed light on the underlying mechanisms of photocatalytic reactions but also pave the way for realizing systematically designed, novel photochemical processes. Moreover, the remarkable photocatalytic capabilities of our indole-fused polycyclic organoPCs hold significant promise for their use in other valuable photochemical reactions.

Data availability

The data underlying this study are available in the published article and its ESI.† Crystallographic data for **A** have been deposited at the CCDC2225142.

Author contributions

Y. L., B. H. J., S. W., S. K., and J. B. performed synthetic and mechanistic studies. Y. Y. and E. J. C. coordinated the experiments and analyses. All authors analyzed the experimental data and wrote the manuscript.

Conflicts of interest

The authors declare no competing financial interest.

Acknowledgements

References

1 N. Hoffmann, Photochemical cycloaddition between benzene derivatives and alkenes, *Synthesis*, 2004, **4**, 481–495.

2 N. Hoffmann, Photochemical reactions as key steps in organic synthesis, *Chem. Rev.*, 2008, **108**, 1052–1103.

3 C. Roscini, K. L. Cubbage, M. Berry, A. J. Orr-Ewing and K. I. Booker-Milburn, Reaction Control in Synthetic Organic Photochemistry: Switching between [5+2] and [2+2] Modes of Cycloaddition, *Angew. Chem., Int. Ed.*, 2009, **48**, 8716–8720.

4 S. Poplata, A. Troster, Y. Q. Zou and T. Bach, Recent Advances in the Synthesis of Cyclobutanes by Olefin [2 + 2] Photocycloaddition Reactions, *Chem. Rev.*, 2016, **116**, 9748–9815.

5 D. Sarkar, N. Bera and S. Ghosh, [2+2] Photochemical cycloaddition in organic synthesis, *Eur. J. Org Chem.*, 2020, **2020**, 1310–1326.

6 M. Sicignano, R. I. Rodríguez and J. Alemán, Recent Visible Light and Metal Free Strategies in [2+2] and [4+2] Photocycloadditions, *Eur. J. Org Chem.*, 2021, **2021**, 3303–3321.

7 P. Franceschi, S. Cuadros, G. Goti and L. Dell'Amico, Mechanisms and Synthetic Strategies in Visible Light-Driven [2+2]-Heterocycloadditions, *Angew. Chem., Int. Ed.*, 2023, **62**, e202217210.

8 P. Xiong, S. I. Ivlev and E. Meggers, Photoelectrochemical asymmetric dehydrogenative [2+2] cycloaddition between C–C single and double bonds via the activation of two $C(sp^3)$–H bonds, *Nat. Catal.*, 2023, **6**, 1–8.

9 C. R. Stephenson, T. P. Yoon and D. W. C. MacMillan, *Visible light photocatalysis in organic chemistry*, John Wiley & Sons, 2018.

10 L. Marzo, S. K. Pagire, O. Reiser and B. König, Visible-light photocatalysis: does it make a difference in organic synthesis?, *Angew. Chem., Int. Ed.*, 2018, **57**, 10034–10072.

11 S. A. Younis, E. E. Kwon, M. Qasim, K. H. Kim, T. Kim, D. Kukkar, X. M. Dou and I. Ali, Metal-organic framework as a photocatalyst: progress in modulation strategies and environmental/energy applications, *Prog. Energy Combust. Sci.*, 2020, **81**, 100870.

12 M. J. Genzink, J. B. Kidd, W. B. Swords and T. P. Yoon, Chiral Photocatalyst Structures in Asymmetric Photochemical Synthesis, *Chem. Rev.*, 2022, **122**, 1654–1716.

13 L. Buglioni, F. Raymenants, A. Slattery, S. D. A. Zondag and T. Noël, Technological Innovations in Photochemistry for Organic Synthesis: Flow Chemistry, High-Throughput Experimentation, Scale-up, and Photoelectrochemistry, *Chem. Rev.*, 2022, **122**, 2752–2906.

14 F. Strieth-Kalthoff, M. J. James, M. Teders, L. Pitzer and F. Glorius, Energy transfer catalysis mediated by visible light: principles, applications, directions, *Chem. Soc. Rev.*, 2018, **47**, 7190–7202.

15 Q. Q. Zhou, Y. Q. Zou, L. Q. Lu and W. J. Xiao, Visible-Light-Induced Organic Photochemical Reactions through Energy-Transfer Pathways, *Angew. Chem., Int. Ed.*, 2019, **58**, 1586–1604.

16 F. Strieth-Kalthoff and F. Glorius, Triplet Energy Transfer Photocatalysis: Unlocking the Next Level, *Chem*, 2020, **6**, 1888–1903.

17 J. Großkopf, T. Kratz, T. Rigotti and T. Bach, Enantioselective Photochemical Reactions Enabled by Triplet Energy Transfer, *Chem. Rev.*, 2022, **122**, 1626–1653.

18 D. S. Lee, V. K. Soni and E. J. Cho, N-O Bond Activation by Energy Transfer Photocatalysis, *Acc. Chem. Res.*, 2022, **55**, 2526–2541.

19 A. Palai, P. Rai and B. Maji, Rejuvenation of dearomative cycloaddition reactions via visible light energy transfer catalysis, *Chem. Sci.*, 2023, **14**, 12004–12025.

20 S. Dutta, J. E. Erchinger, F. Strieth-Kalthoff, R. Kleinmans and F. Glorius, Energy transfer photocatalysis: exciting modes of reactivity, *Chem. Soc. Rev.*, 2024, **53**, 1068–1089.

21 J. M. Narayanam and C. R. J. Stephenson, Visible light photoredox catalysis: applications in organic synthesis, *Chem. Soc. Rev.*, 2011, **40**, 102–113.

22 C. K. Prier, D. A. Rankic and D. W. C. MacMillan, Visible light photoredox catalysis with transition metal complexes: applications in organic synthesis, *Chem. Rev.*, 2013, **113**, 5322–5363.

23 T. Zhang, Y. Zhang and S. Das, Deal;Photoredox Catalysis for the Cycloaddition Reactions, *ChemCatChem*, 2020, **12**, 6173–6185.

24 N. L. Reed and T. P. Yoon, Oxidase reactions in photoredox catalysis, *Chem. Soc. Rev.*, 2021, **50**, 2954–2967.

25 N. Holmberg-Douglas and D. A. Nicewicz, Photoredox-Catalyzed C-H Functionalization Reactions, *Chem. Rev.*, 2022, **122**, 1925–2016.

26 S. P. Pitre and L. E. Overman, Strategic Use of Visible-Light Photoredox Catalysis in Natural Product Synthesis, *Chem. Rev.*, 2022, **122**, 1717–1751.

27 N. A. Romero and D. A. Nicewicz, Organic Photoredox Catalysis, *Chem. Rev.*, 2016, **116**, 10075–10166.

28 L. Buzzetti, G. E. M. Crisenza and P. Melchiorre, Mechanistic Studies in Photocatalysis, *Angew. Chem., Int. Ed.*, 2019, **58**, 3730–3747.

29 M. Bera, D. S. Lee and E. J. Cho, Advances in N-centered intermediates by energy transfer photocatalysis, *Trends Chem.*, 2021, **3**, 877–891.

30 N. E. S. Tay, D. Lehnherr and T. Rovis, Photons or Electrons? A Critical Comparison of Electrochemistry and Photoredox Catalysis for Organic Synthesis, *Chem. Rev.*, 2022, **122**, 2487–2649.

31 H. Jung, M. Hong, M. Marchini, M. Villa, P. S. Steinlandt, X. Huang, M. Hemming, E. Meggers, P. Ceroni, J. Park and M. H. Baik, Understanding the mechanism of direct visible-light-activated [2 + 2] cycloadditions mediated by Rh and Ir photocatalysts: combined computational and spectroscopic studies, *Chem. Sci.*, 2021, **12**, 9673–9681.

32 S. Bouayad-Gervais, C. D.-T. Nielsen, A. Turksoy, T. Sperger, K. Deckers and F. Schoenebeck, Access to Cyclic N-Trifluoromethyl Ureas through Photocatalytic Activation of Carbamoyl Azides, *J. Am. Chem. Soc.*, 2022, **144**, 6100–6106.

33 N. E. S. Tay, K. A. Ryu, J. L. Weber, A. K. Olow, D. C. Cabanero, D. R. Reichman, R. C. Oslund, O. O. Fadeyi and T. Rovis, Targeted activation in localized protein environments via deep red photoredox catalysis, *Nat. Chem.*, 2023, **15**, 101–109.

34 J. Bae, N. Iqbal, H. S. Hwang and E. J. Cho, Sustainable preparation of photoactive indole-fused tetracyclic molecules: a new class of organophotocatalysts, *Green Chem.*, 2022, **24**, 3985–3992.

35 J. Bae and E. J. Cho, P, N Ligand in Ni-Catalyzed Cross-Coupling Reactions: A Promising Tool for π-Functionalization, *ACS Catal.*, 2023, **13**, 13540–13560.

36 N. Salaverri, J. Alemán and L. Marzo, Harnessing the Power of the De Mayo Reaction: Unveiling a Photochemical and Photocatalytic Masked [2+2] Methodology for Organic Synthesis, *Adv. Synth. Catal.*, 2024, **366**, 156–167.

37 P. De Mayo, H. Takeshita and A. B. M. A. Sattar, The photochemical synthesis of 1,5-diketones and their cyclisation: a new annulation process, *Proc. Chem. Soc.*, 1962, **1962**, 119.

38 P. De Mayo and H. Takeshita, Photochemical syntheses 6. The formation of heptandiones from acetylacetone and alkenes, *Can. J. Chem.*, 1963, **41**, 440–449.

39 D. Tymann, D. C. Tymann, U. Bednarzick, L. Iovkova-Berends, J. Rehbein and M. Hiersemann, Development of an Alkyne Analogue of the de Mayo Reaction: Synthesis of Medium-Sized Carbacycles and Cyclohepta[b]indoles, *Angew. Chem., Int. Ed.*, 2018, **57**, 15553–15557.

40 R. Martinez-Haya, L. Marzo and B. König, Reinventing the De Mayo reaction: synthesis of 1,5-diketones or 1,5-ketoesters via visible light [2+2] cycloaddition of beta-diketones or beta-ketoesters with styrenes, *Chem. Commun.*, 2018, **54**, 11602–11605.

41 The Marzo and Alemán group previously reported a DeMayo-type process employing [Ir{dF(CF$_3$)ppy}$_2$(bpy)]PF$_6$ in the presence of DBU in THF, see: N. Salaverri, R. Mas-Ballesté, L. Marzo and J. Alemán, Visible light mediated photocatalytic [2 + 2] cycloaddition/ring-opening rearomatization cascade of electron-deficient azaarenes and vinylarenes, *Commun. Chem.*, 2020, **3**, 132.

42 T. O. Paulisch, L. A. Mai, F. Strieth-Kalthoff, M. J. James, C. Henkel, D. M. Guldi and F. Glorius, Dynamic Kinetic Sensitization of β-Dicarbonyl Compounds-Access to Medium-Sized Rings by De Mayo-Type Ring Expansion, *Angew. Chem., Int. Ed.*, 2022, **61**, e202112695.

43 W. Zhang and S. Luo, Visible-light promoted de Mayo reaction by zirconium catalysis, *Chem. Commun.*, 2022, **58**, 12979–12982.

44 R. M. Kelch, A. Whyte, E. Lee and T. P. Yoon, Investigating the Effect of Lewis Acid Co-catalysts on Photosensitized Visible-Light De Mayo Reactions, *Org. Lett.*, 2023, **25**, 4098–4102.

45 The photocatalytic reactivity originated from the core polycyclic structure. In the transformation, the alkenyl substituent of the organoPC did not affect the photocatalytic reactivity (see Fig. S15† for more details).

46 X. H. Ma, J. Li, P. Luo, J. H. Hu, Z. Han, X. Y. Dong, G. Xie and S. Q. Zang, Carbene-stabilized enantiopure heterometallic clusters featuring EQE of 20.8% in circularly-polarized OLED, *Nat. Commun.*, 2023, **14**, 4121.

47 J. Ma, S. Chen, P. Bellotti, R. Guo, F. Schafer, A. Heusler, X. Zhang, C. Daniliuc, M. K. Brown, K. N. Houk and F. Glorius, Photochemical intermolecular dearomative cycloaddition of bicyclic azaarenes with alkenes, *Science*, 2021, **371**, 1338–1345.

48 S. Kim, H. J. Bae, S. Park, W. Kim, J. Kim, J. S. Kim, Y. Jung, S. Sul, S. G. Ihn, C. Noh, S. Kim and Y. You, Degradation of blue-phosphorescent organic light-emitting devices involves exciton-induced generation of polaron pair within emitting layers, *Nat. Commun.*, 2018, **9**, 1211.

49 Y. K. Moon, H. J. Jang, S. Hwang, S. Kang, S. Kim, J. Oh, S. Lee, D. Kim, J. Y. Lee and Y. You, Modeling Electron-Transfer Degradation of Organic Light-Emitting Devices, *Adv. Mater.*, 2021, **33**, e2003832.

50 S. Lee, Y. You, K. Ohkubo, S. Fukuzumi and W. Nam, Highly efficient cycloreversion of photochromic dithienylethene compounds using visible light-driven photoredox catalysis, *Chem. Sci.*, 2014, **5**, 1463–1474.

51 In this chemical process, the likelihood of the fully conjugated quinoid form, which exists in equilibrium with **1**, is expected to increase in the presence of **A**. This increase can be attributed to the superior π–π interaction between **A** and the quinoid. Consequently, the reaction with **A** does not necessitate the addition of any base to facilitate the formation of quinoid form.

52 P. Bellotti and F. Glorius, Strain-Release Photocatalysis, *J. Am. Chem. Soc.*, 2023, **145**, 20716–20732.

53 E. J. Cho, Radical-Mediated Fluoroalkylations, *Chem. Rec.*, 2016, **16**, 47–63.

54 T. Chatterjee, N. Iqbal, Y. You and E. J. Cho, Controlled Fluoroalkylation Reactions by Visible-Light Photoredox Catalysis, *Acc. Chem. Res.*, 2016, **49**, 2284–2294.

55 C. H. Ka, S. Kim and E. J. Cho, Visible Light-Induced Metal-Free Fluoroalkylations, *Chem. Rec.*, 2023, **23**, e202300036.